Effect of Particle-Size Distribution on the Properties of High-Volume-Fraction SiC_p-Al–Based Composites

CHANG-YOU CHEN and CHUEN-GUANG CHAO

High-volume-fraction SiC-Al–based composites have been fabricated by squeeze casting. The effect of particle-size distribution and squeeze-cast parameters on the metal-matrix composites (MMCs) was investigated. The results showed that bulk density of the composites was 2.855 to 3.067 g/cm^3 with the various component mixtures of SiC particulates, *i.e.*, the SiC volume fraction was 51.6 to 74.4 pct. The young's modulus of the composites was between 220 and 226 GPa. The maximum four-point bending strength and fracture toughness reached 478 MPa and 9.42 MPa(m)$^{-1/2}$, respectively. The coefficient of thermal expansion (CTE) of the composites was from 5 to 8 $\times$ 10^{-6}/K, depending on the volume fraction of SiC.

I. INTRODUCTION

PARTICULATE silicon carbide–reinforced metal-matrix composites (MMCs) have a high potential for advanced engineered materials that have been developed and recently qualified for use in aerospace structures, inertial guidance systems,[1] and lightweight optical assemblies.[2,3,4] Such materials generally exhibit greater a Young's modulus, higher strengths, and better resistance to creep than the unreinforced alloy; they can also be tailored to match the coefficients of thermal expansion (CTEs) of other materials, including stainless steel, silicon wafers, aluminaum, *etc.*[5,6,7]

Many different technologies for production of SiC/Al composites have emerged over the years. A few of these evolved from methods originally developed for structural applications wherein the amount of SiC particulate was restricted to volume fractions of 0.15 to 0.25, while some are more suited for the higher particulate volume fractions required for optimum CTE matching to optical assembly materials. The powder-metallurgy (PM) process is based on well-established technology[8,9] whereby the SiC particulates are blended with aluminum powder and then consolidated into a fully dense product by vacuum hot pressing. A limitation of this approach is that the maximum volume fraction of SiC particulates that can be incorporated is 0.5 to 0.55, thus placing a limit on the CTE reduction achievable. Some other drawbacks of the process include relatively high costs due to the variety of processing steps involved in the production of a fully dense product, as well as the need for subsequent machining of the final component from the forged or extruded stock.

Casting processes, which include pressureless infiltration,[10] gas-pressure infiltration,[11,12,13] and squeeze casting,[14,15] have been utilized to achieve a high volume fraction of SiC reinforcement levels. A primary drawback of pressureless infiltration is believed to be the need to use specific Al-Mg alloy compositions and a nitrogen-protecting furnace during heating, in order to allow the molten alloy to effectively wet and, thus, infiltrate the SiC. Additionally, since the infiltration relies solely on capillary action, it is possible that certain locations of the preform will be incompletely infiltrated. Squeeze casting is a method that applies pressure to push molten alloy into preforms made of ceramic particle. Preforms can be manufactured by a number of known ceramic processing routes, including injection molding, dry pressing, and slip casting. Several studies have presented information on MMCs produced by the squeeze-casting process.[14,15] Most reports investigated the effect of reinforcements that have monosized particles on the properties of MMCs. Lewis and Goldman[16] argued that a large difference in particle sizes aids in packing. For a high packing density, the particle-size distribution has a large spread. However, few studies have reported on the effect of multimodal powders on the properties of MMCs. In the present work, we choose multimodal SiC powder and different pressures to manufacture high-volume-fraction SiC/Al composites. We also study the effects of particle-size distribution and squeeze-cast parameters on the properties of MMCs.

II. EXPERIMENTAL PROCEDURE

Silicon carbide powders of different particle sizes were used in the present experiment. The particle sizes ranged from 1 to 125 μm and were divided into 11 levels (1, 2, 5, 7.5, 13, 15, 19, 25, 38, 46, and 125 μm average sizes). The matrix alloy was A356. The properties of both SiC and A356 are listed in Table I. The MMCs were fabricated by squeeze casting. Sixty grams of SiC particles, which included varied ratios of different-sized particles, were blended by using a rotating cylindrical container. The blended powder was put into a 5-cm-diameter cylindrical mold and was compacted by hydraulic pressure. The compacted pressure was varied from 25 to 200 MPa (25, 50, 100, 150 and 200 MPa). The mold was preheated to 555 °C. The liquid aluminum alloy, at 750 °C, was squeezed into the same mold as the compaction mold by using the same pressure as the compact pressure. The punch speed was 2 mm/s and the holding time was 120 seconds. A quantitative analysis of microstructure and porosity was obtained from an optical microscope and image analyzer.

The apparent and bulk densities were determined by Archimedes' principle, where the weight of the specimen in air was compared to its weight suspended in water. The

CHANG-YOU CHEN, Graduate Postdoctoral Candidate Student, and CHUEN-GUANG CHAO, Professor, are with the Department of Materials Science and Engineering, National Chiao Tung University, Hsinchu, Taiwan 30049, Republic of China.

Manuscript submitted July 26, 1999.

Table I. The Properties of SiC and A356 Alloy

Properties Materials	Density (g/cm^3)	Young's Modulus (GPa)	CTE ($10^{-6}/K$)
SiC	3.2	400 to 440	3.4
A356	2.68	72	21.5 to 23.5

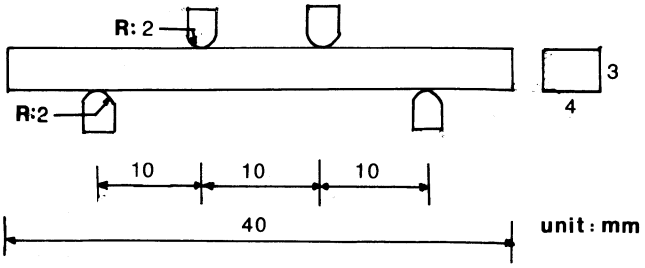

Fig. 1—Dimension of four-point bending specimens.

procedure involved first measuring the dry weight (D). The specimen was then boiled in water for 2 hours and then allowed to cool in the water for 24 hours. The purpose is to eliminate the air in the open pores of the specimen. The wet weight in air (W) and the wet weight suspended in water (S) were then measured. The apparent and bulk densities are given by Eqs. [1] and [2]:

$$\text{apparent density} = D/(D - S) \cdot 1 \text{ (in g/cm}^3\text{)} \quad [1]$$

$$\text{bulk density} = D/(W - S) \cdot 1 \text{ (in g/cm}^3\text{)} \quad [2]$$

The Young's modulus was measured by an ES3000 Elasto Sonic tester and is given by Eq. [3].

$$\text{Young's modulus} = KMFL^3/WH^3 \text{ (in GPa)} \quad [3]$$

where L represents the length of specimen, M is the mass of the specimen, W is the width of the specimen, F is the natural frequency, H is the height of the sample, and K is a constant.

The bending rupture stress was carried out by a four-point test, according to the JIS R1601 specification shown in Figure 1.

$$\text{The bending strength} = 3P(L - 1)/2wt^2 \text{ (in kg/mm}^2\text{)}$$

where P represents the load, w represents width of the specimen, and t represents the thickness of the specimen.

A thermal-expansion analysis was run by using a DUPONT* thermal analysis-TMA 2940 system. The tests were conducted on rectangular specimens measuring 3 × 4 × 18 mm. The heating rate was 5 °C/min from room temperature to 500 °C. Dry nitrogen was purged through the furnace at the rate of 100 mL/min.

*DUPONT is a trademark of E. I. DuPont de Nemours, Wilmington, DE.

The fracture toughness was measured by the single-edged notch-beam (SENB) method. The shape of the specimen is shown in Figure 2. The fracture toughness (K_Q) is calculated by Eq. [4].

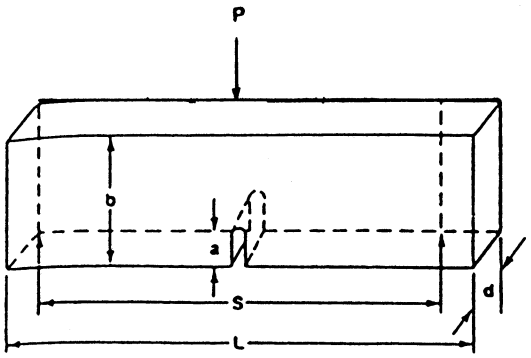

Fig. 2—The shape and dimension of single-edged notch-beam specimen.

$$K_1 = \frac{0.4744P}{db^2}\frac{\sqrt{a}}{1}\left(1.93 - 3.07\left(\frac{a}{b}\right) + 14.53\left(\frac{a}{b}\right)^2 - 25.11\left(\frac{a}{b}\right)^3 + 25.80\left(\frac{a}{b}\right)^4\right) \text{ (in MPa(m)}^{-1/2}\text{)} \quad [4]$$

where the P is the load, b is the thickness of the specimen, a is the depth of the precrack, and d is the width of the specimen.

The fracture-toughness tests were carried out in an Instron machine with a 0.5 mm/min crosshead speed. The specimens were fatigue precracked. To ensure that cracking occurred correctly, the specimens contained starter notches, which were 0.15 mm wide and 1.3 mm deep. At least three samples were measured for each kind of test.

III. RESULTS

A. *Microstructural Examination*

The components of the multimodal powder and the volume fraction of the MMCs are listed in Table II. The bulk density included closed pores and open pores. The apparent density included only closed pores. Both the bulk density and the apparent density are almost the same in specimens 1 through 6. It means that the porosity of specimens opened to the surface is very low. Figures 3(a) through (f) illustrate the photomicrographs of specimens 1 through 6, showing a homogenous distribution of particles and few pores. The results show that the internal porosity of the specimen is also low. Specimens 7 through 10 have the same ratio of particle sizes, but each particle size is reduced by two thirds relative to specimens 1 through 4, respectively. Specimens 7 through 10 have a lower volume fraction and higher porosity than specimens 1 through 4. The photomicrographs of specimens 7 through 10 show that the porosity apparently increases (Figures 4(a) through (d)).

B. *The Influence of Pressure*

Figure 5 shows the relationship between the volume fraction of SiC particles and squeezed pressure. The volume fraction increases with increasing squeezed pressure. Figure 6 shows the photomicrographs of specimens 11 through 14

Table II. The Characteristics of Multimodal Packing of All the Specimens

Packing Specimen	Characteristic Component Ratio	Squeeze Pressure (MPa)	Bulk Density (ρb)	Apparent Density (ρa)	$\frac{\rho a - \rho b}{\rho b}$ (Pct)	Volume Fraction V_f (Pct)	Porosity (Pct)
1	(125 μ) 25 pct (46 μ) 25 pct (19 μ) 25 pct (13 μ) 25 pct	50	2.988	2.989	0.03	59.4	<1
2	(125 μ) 30 pct (46 μ) 30 pct (25 μ) 40 pct	50	2.994	2.996	0.07	60.5	<1
3	(125μ) 50 pct (46 μ) 25 pct (25 μ) 10 pct (15 μ) 10 pct (7.5 μ) 5 pct	50	3.039	3.041	0.07	69.2	<1
4	(125 μ) 50 pct (38 μ) 15 pct (13 μ) 15 pct (7.5 μ) 20 pct	50	3.032	3.035	0.1	67.8	<1
5	(125 μ) 25 pct (83 μ) 25 pct (38 μ)10 pct (13 μ) 10 pct (5 μ) 20 pct (1 μ) 10 pct	50	3.030	3.032	0.07	67.5	<1
6	(125 μ) 50 pct (38 μ) 25 pct (19 μ) 15 pct (7.5 μ) 10 pct	50	3.043	3.045	0.07	70.0	<1
7	(38 μ) 50 pct (15 μ) 25 pct (7.5 μ) 25 pct (5 μ) 25 pct	50	2.862	2.874	0.4	51.6	3.2
8	(38 μ) 30 pct (15 μ) 30 pct (7.5 μ) 40 pct	50	2.855	2.869	0.5	58.5	4.8
9	(38 μ) 50 pct (15 μ) 25 pct (7.5 μ) 10 pct (5 μ) 10 pct (2 μ) 5 pct	50	2.998	2.999	0.03	63.7	<1
10	(38 μ) 50 pct (13 μ) 15 pct (5 μ) 15 pct (2 μ) 20 pct	50	2.999	3.006	0.27	64.7	<1
11	(125 μ) 50 pct (38 μ) 15 pct (13 μ) 15 pct (5 μ) 20 pct	25	2.945	2.957	0.4	63.9	4.2
12	(125 μ) 50 pct (38 μ) 15 pct (13 μ) 15 pct (5 μ) 20 pct	100	3.049	3.053	0.13	71.1	<1
13	(125 μ) 50 pct (38 μ) 15 pct (13 μ) 15 pct (5 μ) 20 pct	150	3.060	3.061	0.03	73.1	<1
14	(125 μ) 50 pct (38 μ) 15 pct (13 μ) 15 pct (5 μ) 20 pct	200	3.067	3.068	0.03	74.4	<1

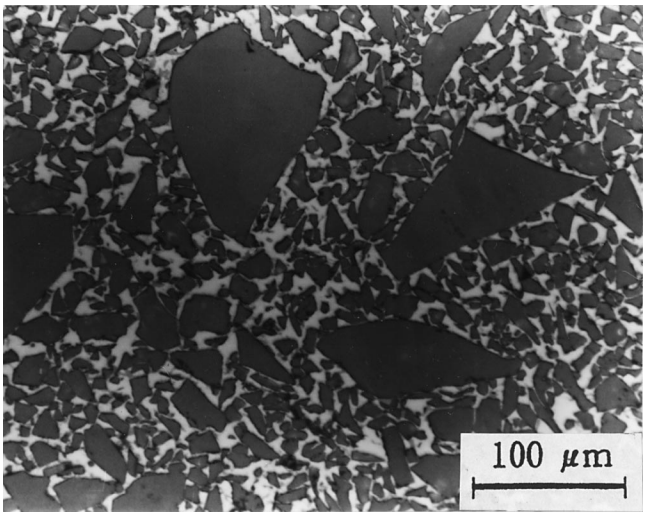

(*a*)

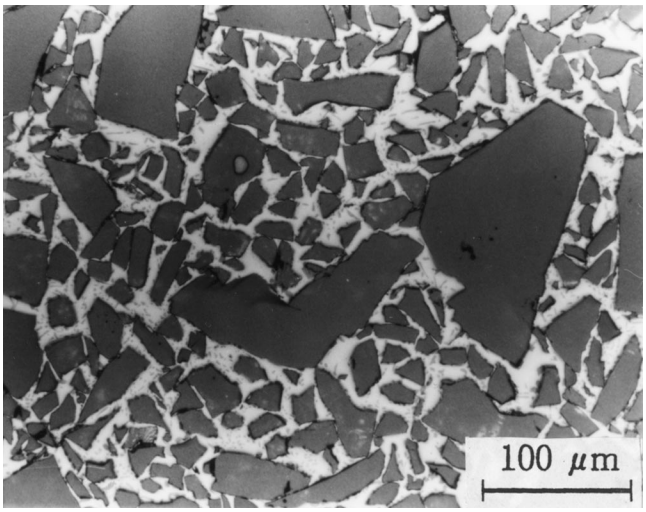

(*b*)

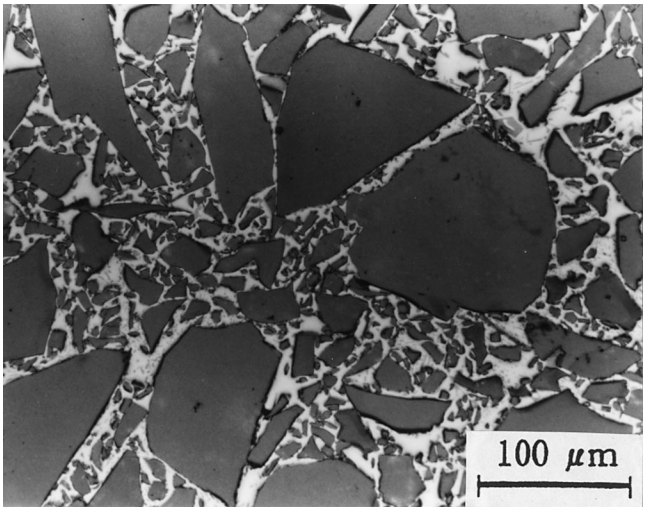

(*c*)

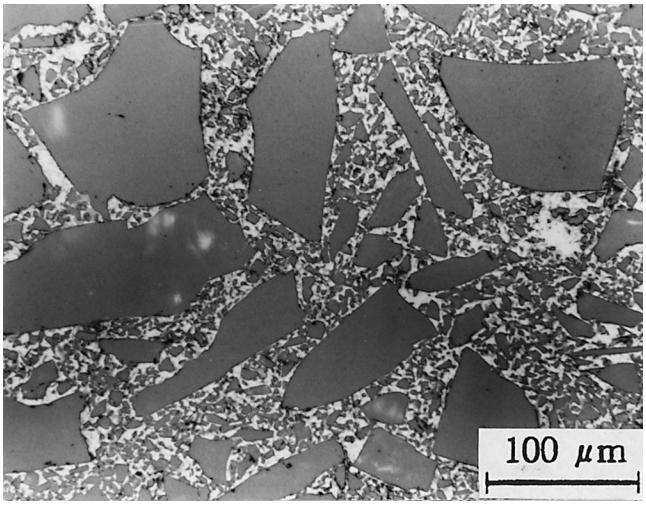

(*d*)

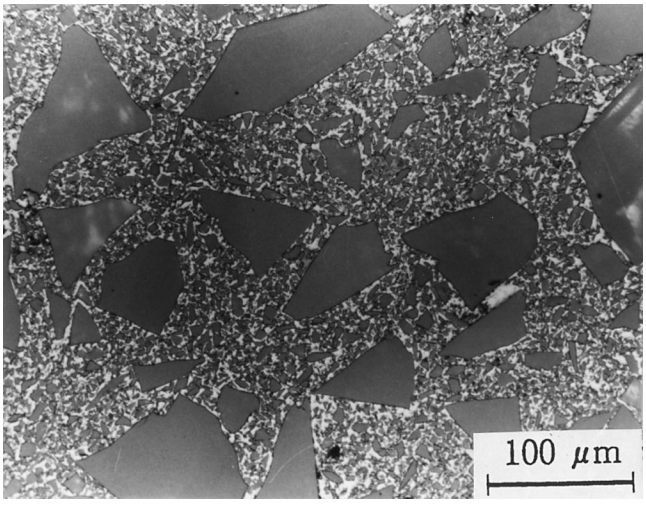

(*e*)

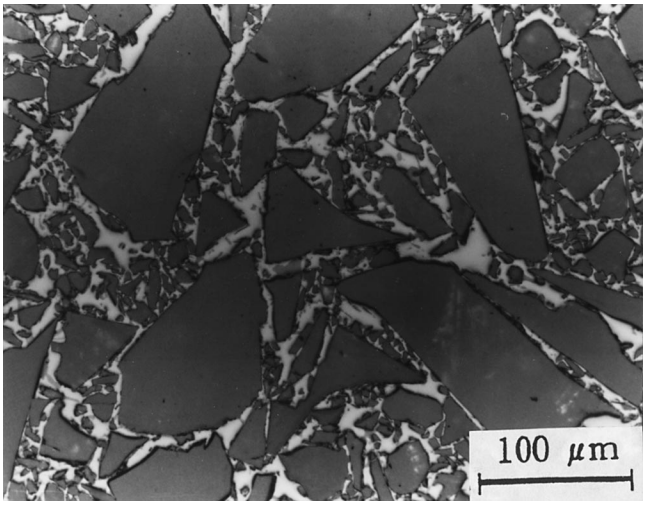

(*f*)

Fig. 3—Photomicrographs of specimens with 50 MPa squeezed pressure: (*a*) specimen 1, (*b*) specimen 2, (*c*) specimen 3, (*d*) specimen 4, (*e*) specimen 5, and (*f*) specimen 6.

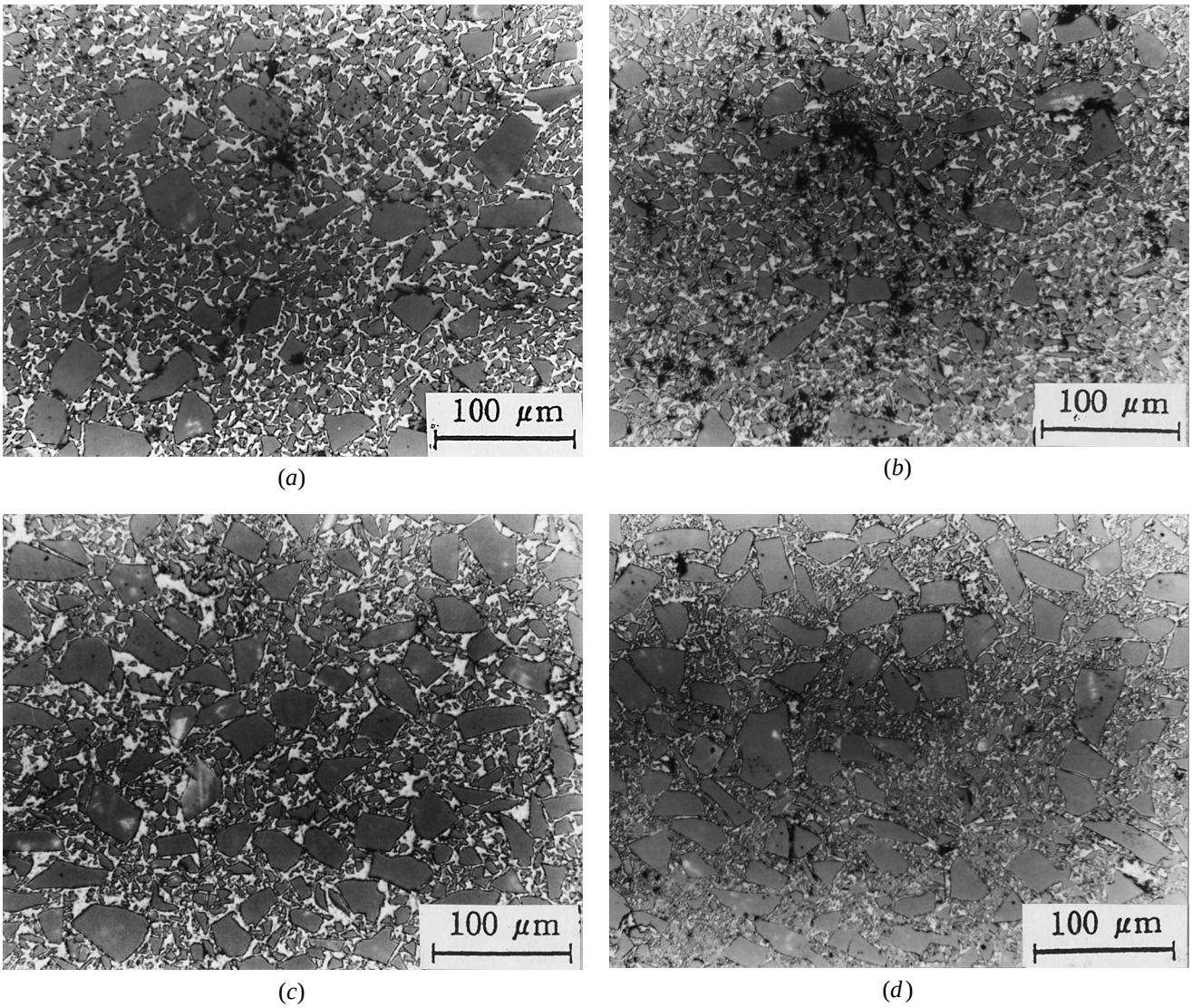

(*a*) (*b*) (*c*) (*d*)

Fig. 4—Photomicrographs of specimens 7 to 10, which have the same ratio of particle sizes, but the particle size is reduced by two thirds relative to specimens 1 through 4, respectively: (*a*) specimen 7, (*b*) specimen 8, (*c*) specimen 9, and (*d*) specimen 10.

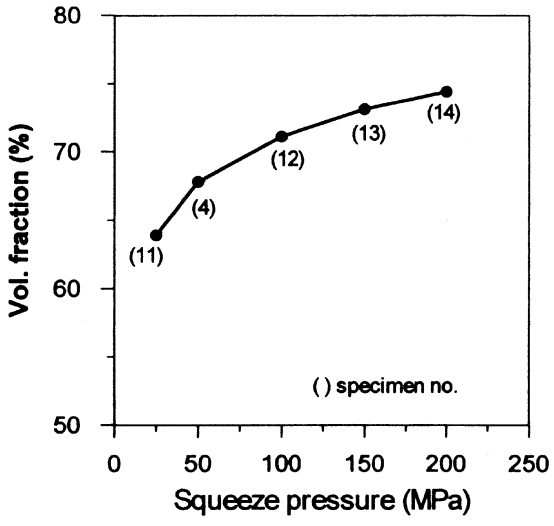

Fig. 5—The relationship between the volume fraction of SiC and squeezed pressure.

with various squeezed pressures. Figure 6(a) illustrates the photomicrograph of specimen 11, which was given 25 MPa of squeezed pressure and shows a lot of porosity.

C. *Mechanical Properties*

Figure 7 shows the relationship between the Young's modulus and the volume fraction of SiC. The Young's modulus slightly increases with increasing volume fraction of SiC. However, the Young's modulus of composites is independent of the particle-size distribution and the squeezed pressure. The Young's-modulus measurements of specimens 7, 8, and 11, which have some porosity, are slightly low. Figure 8(a) shows the effect of squeezed pressure on bending strength with the same particle-size distribution. The bending strength slightly increases with increasing squeeze pressure, except for specimen 11, which has an extremely low strength with 25 MPa of squeeze pressure. Figure 8(b) shows that the relationship between bending strength and volume fraction of particles with various particle-size distributions under the same squeezed pressure (50 MPa). The bending strength is

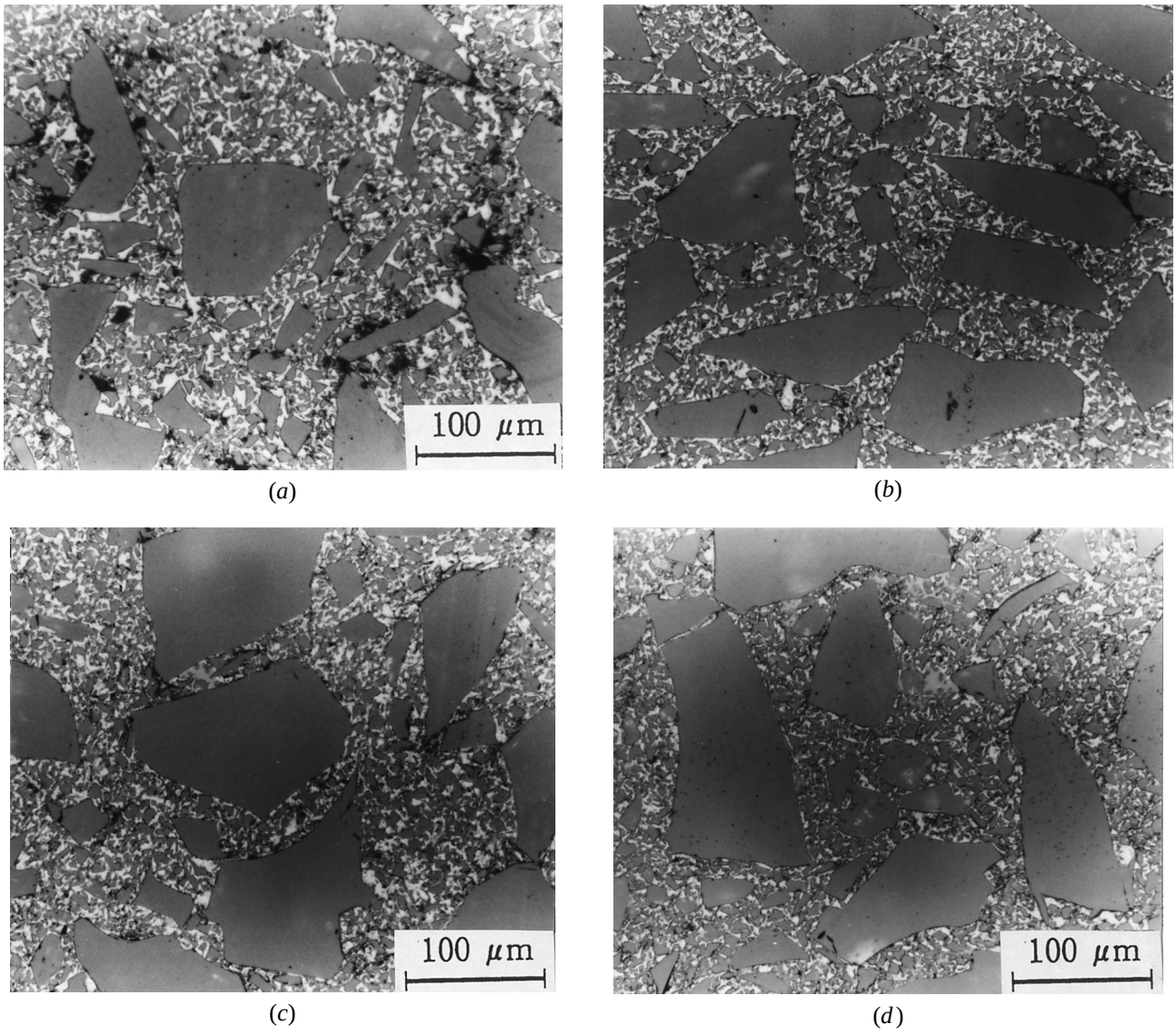

(*a*) (*b*) (*c*) (*d*)

Fig. 6—Photomicrographs of specimens with various squeezed pressures: (*a*) 25 MPa, (*b*) 100 MPa, (*c*) 150 MPa, and (*d*) 200 MPa.

independent of the volume fraction of particles, but dependent on the particle size. Specimens 7 through 10 have the same ratio of particle sizes, but each particle size is reduced by two thirds relative to specimens 1 through 4, respectively. Specimens 9 and 10 have higher bending strengths (478 and 474 MPa, respectively) than specimens 3 and 4 (329 and 364 MPa, respectively). However, specimens 7 and 8, with smaller particle sizes, do not have a higher bending strength, because of a lot of porosity in the composites shown in Figure 4. Figure 9 shows the relationship between fracture toughness and SiC volume fraction. The fracture toughness of the specimens, which have 60 to 70 vol pct SiC, is between 8.40 and 9.42 MPa(m)$^{-1/2}$. The fracture toughness of specimens 7 and 8, which have more porosity, is a lower value of 8.08 and 7.28 MPa(m)$^{-1/2}$, respectively.

D. *The Coefficient of Thermal Expansion*

Figure 10 shows the relationship between the CTE and SiC volume fraction. The average CTE decreases with increasing SiC volume fraction and also decreases with decreasing temperature.

IV. DISCUSSION

According to German's report,[17] a wide particle-size distribution gives a higher packing density compared to a narrow particle-size distribution for a multimodal powder mixture. A key characteristic of all multidomal powder mixtures is that a large difference in particle size aids packing. Figure 11 shows a sketch of an idealized trimodal powder mixing, where the height indicates the packing density, with an optimal intermediate composition.[17] In addition, Horsfield[18] performed one of the early treatment of multimodal packing. He demonstrated, for a mixture of four or five components, a packing density near 0.85. In this study, the results show the same trend. Specimens 3 through 7, which include over 50 pct large particles (>83 μm) and an appropriately small particle-size ratio, have the higher volume fraction of SiC (>65 pct). Specimens 7 through 10 have the

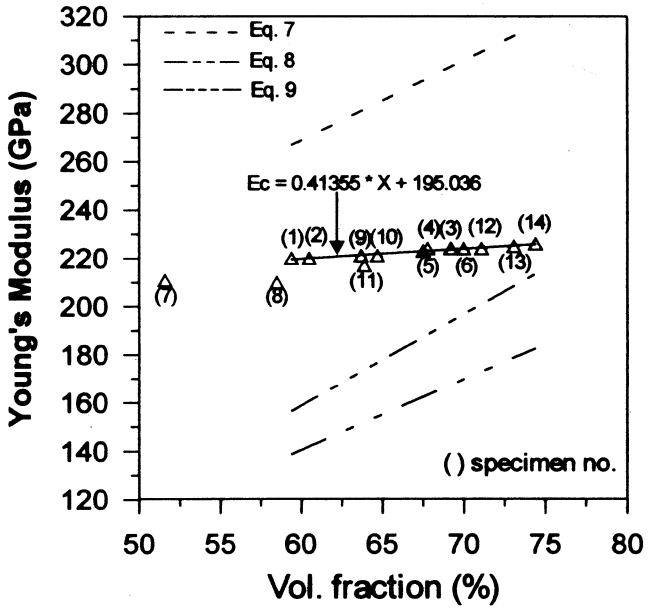

Fig. 7—The relationship between Young's modulus and the volume fraction of SiC.

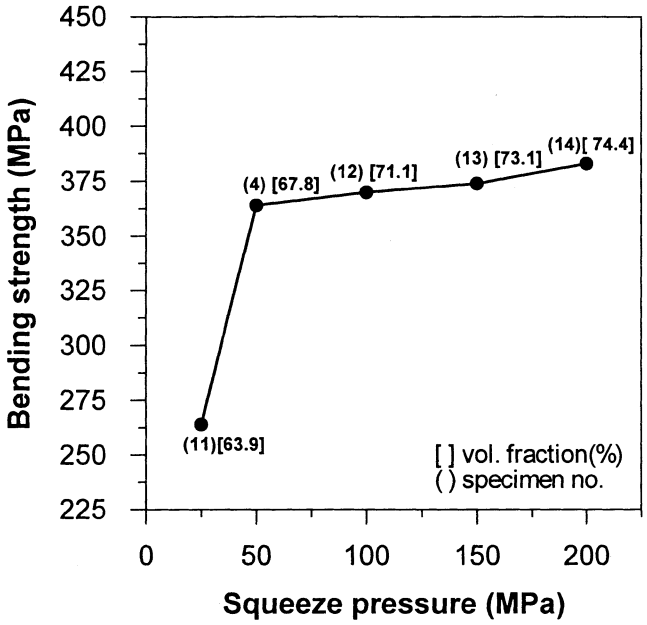

(*a*)

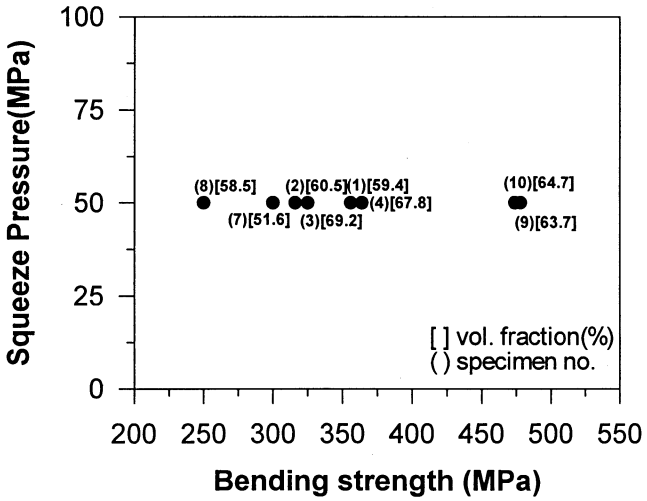

(*b*)

Fig. 8—(*a*) Effect of squeeze pressure on bending strength with the same particle size distribution. (*b*) The relationship between bending strength and volume fraction of particles with various particle size distributions in the same squeezed pressure (50 MPa).

same ratio of particle sizes, but each particle size is reduced by two thirds relative to specimens 1 through 4, respectively. Generally, the smaller particles are more difficult to compact, because of a greater number of contact points and higher stress concentrations at the smaller pores. Since the pore size scales with particle size, compaction of small particles is more difficult. Therefore, specimens 7 through 10 have a lower SiC volume fraction and a higher porosity than specimens 1 through 4. Otherwise, the squeezed pressure is an important factor in fabricating higher volume fractions. For example, in specimen 11, the squeezed pressure of 25 MPa is not high enough to obtain a high volume fraction and no porosity. The volume fraction increases with increasing squeezed pressure. Composites with a high volume fraction and low porosity can be obtained only when the squeezed pressure is more than 50 MPa.

Alan Wolfenden *et al.*[19] reported that the precision for a single measurement of the Young's modulus of 6061Al/SiC*p* by the piezoelectric ultrasonic composite oscillator technique is 0.7 pct. The Young's modulus can be expressed by the following equation:

$$E = 68.6 + 2.2X \quad [5]$$

with $SE = 6.4$ GPa and $R = 0.95$, where X is the volume percent of SiC, SE is the standard error of estimate, and R is the correlation coefficient. In this study, we use a similar technique. The Young's modulus linear increase is attributed to the existence of the second phase (SiC) in the matrix, and that can be expressed by Eq. [6].

$$E = 0.414X + 195 \quad [6]$$

with $R = 0.948$. However, specimens 7 and 8, with a lot of porosity, have a lower Young's modulus. In addition, either a constant stress or a constant strain is assumed, and the resultant properties of the composites can be calculated from the stress-strain properties of the individual phases and volume fractions. The series model assumes that both materials contribute to the composite stiffness in proportion to their respective stiffness and volume fraction:

$$E = E_m f_m + E_r f_r \quad [7]$$

where E_m is the Young's modulus of the matrix, f_m is the volume fraction of the matrix, E_r is the Young's modulus of the reinforcement, and f_r is the volume fraction of the reinforcement. It has been shown that Eq. [7] provides an upper bound for the composite elastic modulus E in those cases where both constituent materials have the same value of Poisson's ratio.[20,21] Another model is the parallel model, which describes the compliance in terms of constituent materials subjected to uniform stress conditions:

$$E = (f_m/E_m + f_r/E_r)^{-1} \quad [8]$$

Equation [8] provides a lower bound for the equivalent

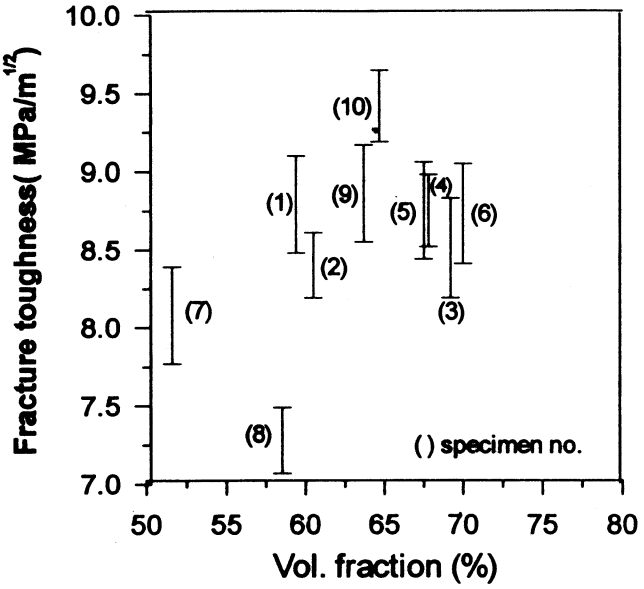

Fig. 9—The relationship between fracture toughness and volume fraction of SiC.

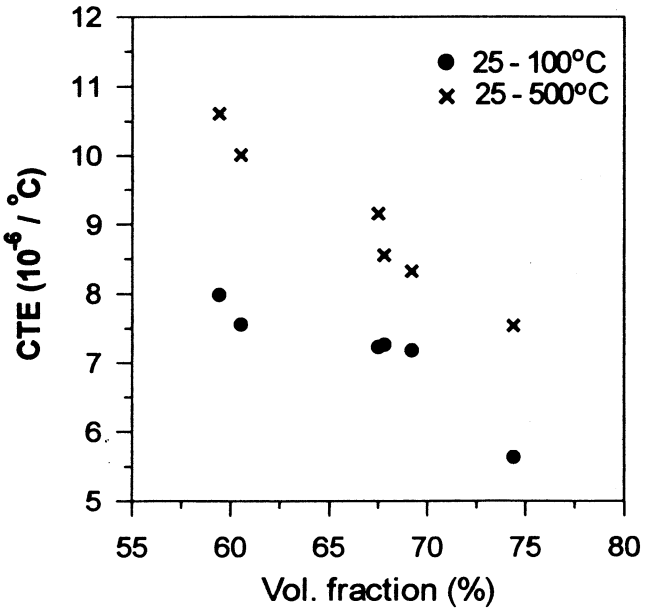

Fig. 10—The relationship between CTE and volume fraction of SiC.

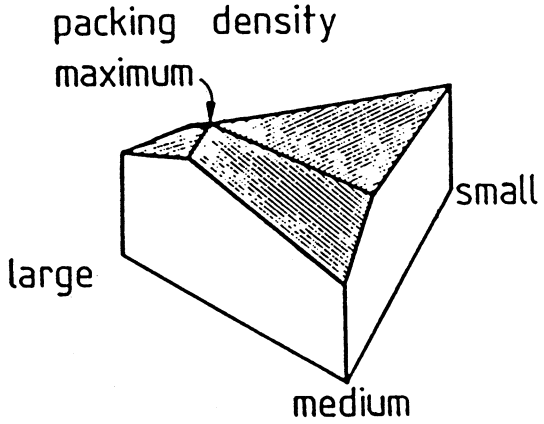

Fig. 11—A sketch of an idealized trimodal powder mixing, where the height indicates the packing density, with an optimal intermediate composition.

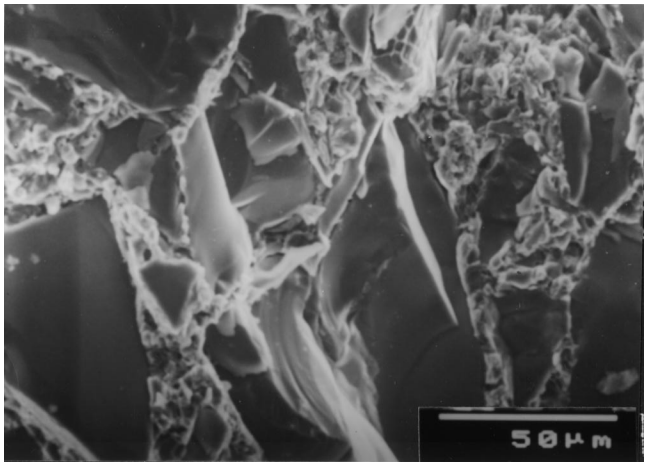

Fig. 12—A micrograph of the fracture surface of the specimen.

elastic modulus E.[20,21] Between the upper and lower bounds of Eqs. [7] and [8], other work has been done to describe more accurately the mechanical properties of composites: for example, the Hashin–Shtrikman model[20] (Eq. [9])

$$E = E_m\,(E_m\,f_m + E_r\,(f_r + 1))/(E_r\,f_m + E_m(f_r + 1)) \qquad [9]$$

In this study, the results show that the Young's modulus is between the upper and lower bounds of Eqs. [7] and [8] in the 60 to 75 SiC vol pct range, since the value of the Poisson's ratio is different between A356 and SiC. However, the reason for the difference in slope is not clear and needs further study.

Figure 8(a) shows that the bending strength of the composites is dependent on squeeze pressure and on SiC volume fraction. The higher the volume fraction of SiC particles with the same particle-size distribution, the higher the bending strength of the composites. Besides, the bending strength of the composites is dependent on the particle size shown in Figure 8(b). Specimens 9 and 10 have particle sizes that are reduced by two thirds, relative to to specimens 3 and 4, have a higher bending strength (478 and 474 MPa,respectively) than that of specimens 3 and 4 (329 and 364 MPa, respectively). The bending stress of SiC is dictated by the longest flaw in the particle, and the probability of finding longer defects increases with the particle size. Thus, large particles are more prone to fail than small ones. In fact, the micrograph of the fracture surface shows that the large SiC particles have a brittle fracture, as shown in Figure 12. Therefore, the smaller the particle size, the higher the bending strength.

The fracture toughness of the specimens is in the range from 8.40 to 9.42 MPa$(m)^{-12}$, as shown in Figure 9. It is noted that the fracture toughness has the same trend: the smaller the particle size, the higher the fracture toughness. The fracture toughness of specimens 9 and 10 (8.86 and 9.42 Mpa$(m)^{-1/2}$, respectively) is higher than that of specimens 3 and 4 (8.51 and 8.75 MPa$(m)^{-1/2}$, respectively). However, the fracture toughness of specimens 7 and 8, which have a lot of porosity, is only 8.01 and 7.28 MPa$(m)^{-1/2}$, respectively.

From the curve shown in Figure 10, the CTE of the composites containing 50 to 75 vol pct SiC is from 5 to 8

$\times 10^{-6}$/K. Metal-matrix composite materials specifically tailored for optimized thermal and physical properties can satisfy the needs of the advanced electronics systems designer. It is well known that the CTE at 300 K is 16.2 $\times 10^{-6}$/K for pure copper, 6.5 $\times 10^{-6}$/K for alumina, and 5.8 $\times 10^{-6}$/K for GaAs. The composites that have an appropriate volume fraction of SiC can easily obtain a CTE closely matching that of electronic-grade materials.

V. CONCLUSIONS

In our present study, the effect of SiC powder-size distribution, powder-compaction, and squeeze-cast parameters on the properties of high-volume-particulate aluminum matrix composites is summarized as follows.

1. The high-volume-fraction (>50 pct) SiC particulate composites can be easily fabricated by squeeze casting with multimodal powders.
2. A squeeze pressure of over 50 MPa is needed to fabricate sound composites.
3. The Young's modulus increases with increasing SiC volume fraction but is independent of powder-size distribution and squeeze pressures. The Young's modulus can be expressed by the equation $E = 195 + 0.424\ X$.
4. The bending strength of the composites increases with decreasing SiC particle size and with increasing squeeze pressure.
5. The maximum fracture toughness of the specimens is 9.42 MPa(m)$^{-1/2}$.
6. The CTE of the composites is from 5 to 8 $\times 10^{-6}$/K, dependent on the volume fraction of SiC.

REFERENCES

1. J.K. Lee, Y.V. Earmme, H.I. Aaronson, and K.C. Russell: *Metall. Trans. A*, 1980, vol. 11A, pp. 1837-847.
2. W.R. Mohn and G.A. Gegel: *Advanced Composites: The Lastest Developments*, Advanced Composites, P. Beardmore and C.F. Johnson, eds., Proc. 2nd Conf. on Advanced Composites, P. Beardmore and C.F. Johnson, eds., ASM INTERNATIONAL, Metals Parks, OH, 1986, pp. 69-73.
3. P. Niskanen and W.R. Mohn: *Adv. Mater. Processes*, 1988, vol. 133 (3), pp. 39-41.
4. W.R. Mohn and D. Vukobratovich: *J. Mater. Eng.*, 1988, vol. 10 (3), pp. 225-235.
5. A.L. Geiger and M. Jackson: *Adv. Mater. Processes*, 1989, vol. 136 (1), pp. 23-30.
6. C. Thaw, R. Minet, J. Zemany, and C. Zweben: *SAMPE J.*, 1987, Nov–Dec., pp. 40-43.
7. T.A. Hahn and R.W. Armstrong: *Int. J. Thermophys.*, 1988, vol. 9 (5), pp. 861-71.
8. D.L. McDanels: *Metall. Trans. A*, 1985, vol. 16A, pp. 1105-15.
9. T.G. Nieh and D.J. Chellmam: *Scripta Metall.*, 1984, vol. 18 p. 925.
10. M.K. Premkumar, W.H. Hunt, Jr., and R.R. Sawtell: *JOM*, 1992, July, pp. 24-29.
11. A.J. Cook and P.S. Werner: *Mater. Sci. Eng. A*, 1991, vol. 24A, pp. 186-206.
12. J. Yang and D.D.L. Chung: *J. Mater. Sci.*, 1989, vol. 24, pp. 3605-12.
13. Shy-Wen Lai and D.D.L. Chung: *J. Mater. Sci.*, 1994, vol. 29, pp. 3128-150.
14. C.R. Cook, D.I. Yun, and W.H. Hunt, Jr.: *Proc. Int. Symp. on Advanced in Cast Reinforced Metal Composites*, ASM, Metal Park, OH, 1988, pp. 195-204.
15. S.K. Verma and J.L. Dorcic: *Proc. Int. Symp. on Advanced in Cast Reinforced Metal Composites*, ASM, Metal Park, OH, 1988, pp. 115-26.
16. H.D. Lewis and A. Golfmsn: *J. Am. Ceramic Soc.*, 1966, vol. 49, pp. 323-27.
17. R.M. German: *Powder Metallurgy Science*, Metal Powder Industrues Federation, Princeton, NJ, 1984, pp. 27-36.
18. H.T. Horsfield: *J. Soc. Chem. Ind.*, 1934, vol. 53, pp. 107T-115T.
19. A. Wolfenden, M.R. Harmouche, and S.V. Hayes: *Testing Technology of Metal Matrix Composites*, ASTM STP 964, P.R. DiGiovanni and N.R. Adsit, eds., ASTM, Philadelphia, PA, 1988, pp. 207-15.
20. Z. Hashin and S. Shtrikman: *J. Mech. Phys. Solids*, 1963, vol. 11, pp. 127-40.
21. B. Paul: *Trans. AIME*, 1960, vol. 218, p. 36.